Reduction of broadband noise in vehicles by means of active feedforward control

Malte Misol[a)]
Thomas Haase[b)]
Hans Peter Monner[c)]
Institute of Composite Structures and Adaptive Systems, German Aerospace Center (DLR)
Braunschweig, Germany

Broadband noise in a vehicle's interior is an important issue because of its negative impact on the passengers' comfort and wellbeing. The perception of this broadband noise can increase due to the use of new, less noisy drive concepts and the accompanying loss of masking noise components. This contribution focuses on the reduction of the transmission of external broadband disturbances through lightweight panel structures (e.g. a car's roof liner or an aircraft sidewall panel) by means of active feedforward control. The aim of this work is to demonstrate the potential and to motivate the implementation of active feedforward (instead of feedback) control for the reduction of broadband noise in vehicles. A new method is introduced to quantify the causality of an active feedforward control system configuration. Simulation results show a similar causality of active single and double panel systems, yet a significantly increased control performance of more than 10 dB in the reduction of the sum of the mean-squared error signals of the active double panel system. The main conclusion of this work is that the transmission of external broadband disturbance sources through double-walled vehicle or aircraft structures can be significantly reduced by the application of active feedforward control.

1 INTRODUCTION

Active noise reduction in vehicles is a research topic for more than two decades. The increasing level of integration of electrical systems in automobiles makes the technology nowadays affordable for the mass market[1]. In principle it must be distinguished between the

[a)] email: malte.misol@dlr.de
[b)] email: thomas.haase@dlr.de
[c)] email: hans.monner@dlr.de

destructive interference of airborne sound (active noise control – ANC) and the reduction of structure-borne sound (active vibration control – AVC, active noise vibration control – ANVC or active structural acoustic control – ASAC). Concerning the algorithms it must be distinguished between active feedback control (FBC) and active feedforward control (FFC).

It must be noted that ANC attracts most attention in automotive-related research and application. Depending on the disturbance source, either FBC algorithms (for broadband disturbances) or FFC algorithms (for tonal disturbances) are applied[2,3,4]. A good overview is provided by Elliott[1]. The application of active FFC for the reduction of broadband noise is rather unusual, although it is possible as shown for example by Oh et al.[5]. In Oh et al. the signals of accelerometers mounted at the wheel suspensions are used as reference signals for the active FFC system. This ANC system achieves local reductions of the interior road noise of 6 dB(A) within the control bandwidth. Publications regarding the application of AVC, ANVC or ASAC in cars are relatively rare. Most of these publications concentrate on active FBC. Dehandschutter and Sas[6] reduce the sound pressure level (SPL) in the passenger cabin by means of vibration absorbers mounted at the vehicle body. The rolling noise was reduced by 6 dB at the position of the driver's ear. In Weyer et al.[7], active electromechanical absorbers are applied to the skin of the car roof. Experiments show tonal SPL reductions of up to 15 dB. Misol et al.[8] reduce the sound radiation of the windshield into the passenger cabin by means of different active control systems. The global vibration reduction of the windshield leads to a reduction of the interior SPL of up to 15 dB.

It becomes clear that broadband active FFC is rarely applied for ANC, ANVC or ASAC systems in automobiles. The reasons for this are diverse and often they can't be denied. It can, however, be expected that the ongoing progress in the state of scientific and technological knowledge and the increasing integration degree of electrical systems in automobiles will permit a future application of technologies that are uneconomic at the present moment. The main goal of this contribution is to motivate the application of broadband active FFC in automobiles. The investigation focuses on the active FFC of the transmission of broadband disturbance sources through single panel and double panel lightweight structures (e.g. the roof liner of a car).

At first, some important aspects of sound transmission through panel structures are discussed in order to demonstrate the physical limitations of passive sound insulation treatments and to underline the benefits of active structural acoustic methods (AVC, ANVC, ASAC). Subsequently, the influencing of the sound transmission through panel structures by means of active FFC and the importance of the parameters coherence and causality is discussed. Terms and methods for the analysis of coherence and causality of active FFC systems are introduced and applied to simulation results of generic active single and active double panel systems. Finally, the disturbance rejection (total power of the error signals) and the causality margin (according to the definition provided in Section 3.3) of the active systems are evaluated for different secondary path runtimes (i.e. fast and slow signal processing).

2 SOUND RADIATION OF LIGHTWEIGHT PANEL STRUCTURES

2.1 Coincidence

Coincidence describes the equivalence of the speed of airborne and structure-borne (bending waves) sound. According to Fahy and Gardonio[9] (p. 287), the fundamental coincidence angular frequency is given by

$$\omega_c = c_0^2 \sqrt{\frac{m}{D}}\,. \tag{1}$$

There, c_0 denotes the speed of sound in air, m is the mass per unit area and D is the bending stiffness.

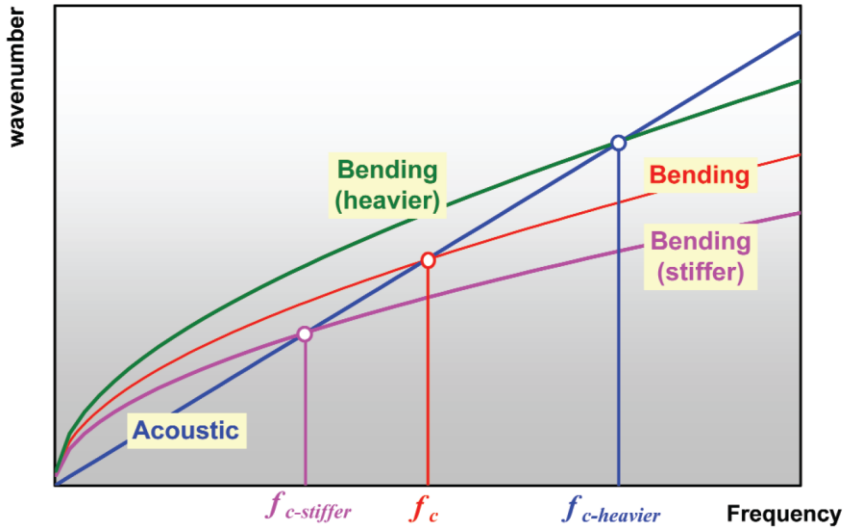

Fig. 1 – Dependency of the coincidence frequency of a panel structure on mass and stiffness. Decrease of the coincidence frequency due to an increase of the stiffness and increase of the coincidence frequency due to an increase in mass[10]

The dependency of the coincidence frequency on mass and stiffness is depicted in Fig. 1 (taken from Hambric and Fahnline[10]). The importance of the coincidence frequency is due to its influence on the sound transmission loss (STL) of panel structures. A disturbance source with a frequency close to the coincidence frequency will induce a strong excitation of the structural dynamics and this will result in a significantly increased sound transmission. Hence, for acoustic reasons, the coincidence frequency should be as high as possible. Equation (1) shows that this comes at the cost of an increase in mass and/or a decrease in bending stiffness of the panel.

2.2 Sound transmission loss of single and double panels

According to Equation (2), the sound transmission through an infinite panel depends on the angle of incidence ϕ of the plane acoustic wave[9] (p. 286). Further parameters are the mass density of air ρ_0, the angular frequency ω, the wavenumber k and the loss factor η.

$$\tau_t(\phi) = \frac{(2\rho_0 c_0 \sec\phi)^2}{[2\rho_0 c_0 \sec\phi + (D/\omega)\eta k^4 \sin^4\phi]^2 + [\omega m - (D/\omega)k^4 \sin^4\phi]^2} \tag{2}$$

At low frequencies ($\omega < \omega_c$) Equation (2) simplifies to

$$\tau_t(\phi) = \frac{1}{[1 + (\omega m \cos\phi/(2\rho_0 c_0))^2]} \,. \tag{3}$$

If $\phi = 0$, i.e. the plane acoustic wave propagates in the direction of the surface normal, the STL can be described by the so-called mass law (or Berger's law).

$$\mathrm{STL}(\phi) = 20\log_{10}\left(\frac{\omega m}{2\rho_0 c_0}\right) \mathrm{dB} \tag{4}$$

According to the mass law, a doubling of mass per unit area or frequency results in an increase in the STL of 6 dB. Hence, the increase of the STL of a panel at low frequencies involves an increase of mass, which runs contrary to the goals of the automotive industry regarding lightweight design and energy efficiency.

The STL of an infinite double panel system excited by a plane wave incident from an angle ϕ (relative to the surface normal) is given by Equation (6). It results from the transmission factor provided by Equation (5)[9] (p. 315ff.).

$$\tau_t(\phi) = \left(\frac{2\rho_0^2 c_0^2 \sec^2\phi \sin(kd\cos\phi)}{\tilde{z}_1'\tilde{z}_2' \sin^2(kd\cos\phi) + \rho_0^2 c_0^2 \sec^2\phi}\right)^2 \tag{5}$$

The impedances $\tilde{z}_i'$ contain the structural and the acoustic wave impedances. Further details and a derivation of Equation (5) can be found in Fahy and Gardonio[9]. Fig. 2 shows the STL of an infinite double panel system according to Equation (6).

$$\mathrm{STL}(\phi) = 10\log_{10}\left(\frac{1}{\tau_t(\phi)}\right) \mathrm{dB} \tag{6}$$

As can be seen in Fig. 2, the STL of a double panel system strongly depends on the mass-air-mass resonance angular frequency ω_0. The fundamental frequency of the mass-air-mass resonance of an infinite, rigid double panel system with enclosed fluid is given by Equation (7).

$$\omega_0 = \left[\left(\frac{\rho_0 c_0^2}{d_{12}}\right)\left(\frac{m_1 + m_2}{m_1 m_2}\right)\right]^{1/2} \tag{7}$$

The symbols m_1 and m_2 denote the panel masses per unit are and d_{12} is the distance between the two panels (see Fig. 3).

Fig. 2 shows the STL of an infinite single and an infinite double panel. At low frequencies ($\omega \ll \omega_0$) where both panels vibrate in phase, the STL of a double panel system equals the STL of a single panel (of equal weight)[9] (p. 307). At frequencies near the mass-air-mass resonance frequency, the panels of the double panel system are strongly coupled through the enclosed air, which leads to a drop in the STL of the double panel system. In this frequency region, the STL is dominated by the

structural damping of the panels and by the acoustic damping of the cavity between the two panels.

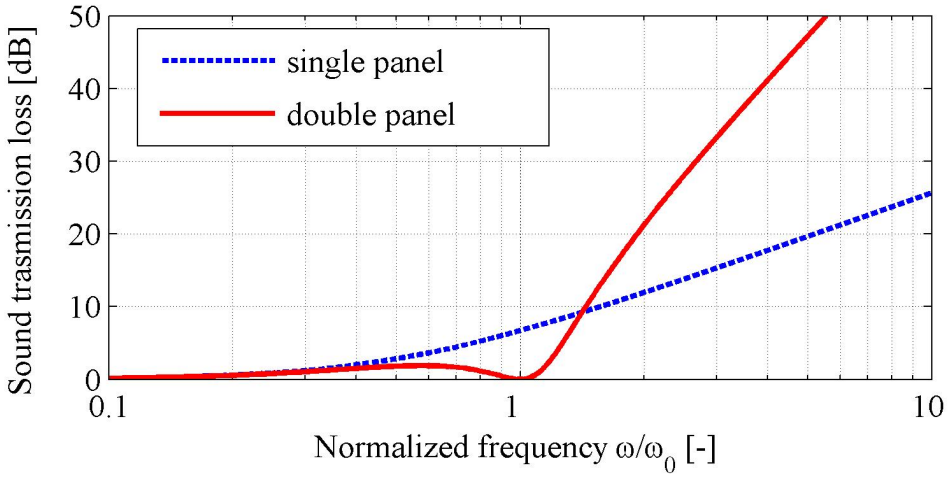

Fig. 2 – Sound transmission loss of an infinite single and an infinite double panel in dependency of the normalized frequency

The coincidence drop of the STL can be weakened by choosing different panel masses. The consequence is a reduction of the STL at higher frequencies[9] (p. 307ff.). Alternatively, if possible, similar panel masses could be chosen in combination with passive or active damping to attenuate the coincidence drop. Usually d_{12} is small compared to the acoustic wavelength in the frequency range of the mass-air-mass resonance frequency (typically around 200 Hz), which limits the effectiveness of passive acoustic cavity damping[9] (p. 311). Active noise reduction systems do not suffer from this restriction, since they perform especially well at low frequencies. Furthermore, the action of a broadband active noise reduction system is not limited to the frequency range around the mass-air-mass resonance frequency. This is very important for broadband disturbances since the resonances of real (finite) structures may lead to additional drops in the STL. The different radiation efficiency of the structural modes makes the non-resonant sound radiation important which raises the need for broadband noise control.

3 INFLUENCING THE SOUND TRANSMISSION LOSS WITH ACTIVE FEEDFORWARD CONTROL

3.1 Principle

Figure 3 shows a sectional drawing of a generic double panel system. The left part of Fig. 3 indicates important vibro-acoustic quantities and the right part of Fig. 3 shows the signals and components of an active FFC system.

Most of the vibro-acoustic quantities indicated in the left part of Fig. 3 had already been defined in the preceding chapter. The primary panel (index 1 – e.g. a skin part of the vehicle body) of the double panel system is excited by the incident sound power $\mathbf{P}_e$ and the secondary panel (index 2 – e.g. an interior panel) radiates the sound power $\mathbf{P}_a$ into the passenger cabin. The stiffness of the structural coupling of the panels is described by k_1 and k_2. Generally, the incident sound power is transmitted via airborne and via structure-borne sound. In the low frequency range, however, most of the incident power is transmitted through the air (see e.g. Tewes[11] on page 76 or Gardonio und Elliott [12] Fig. 7 on page 1030).

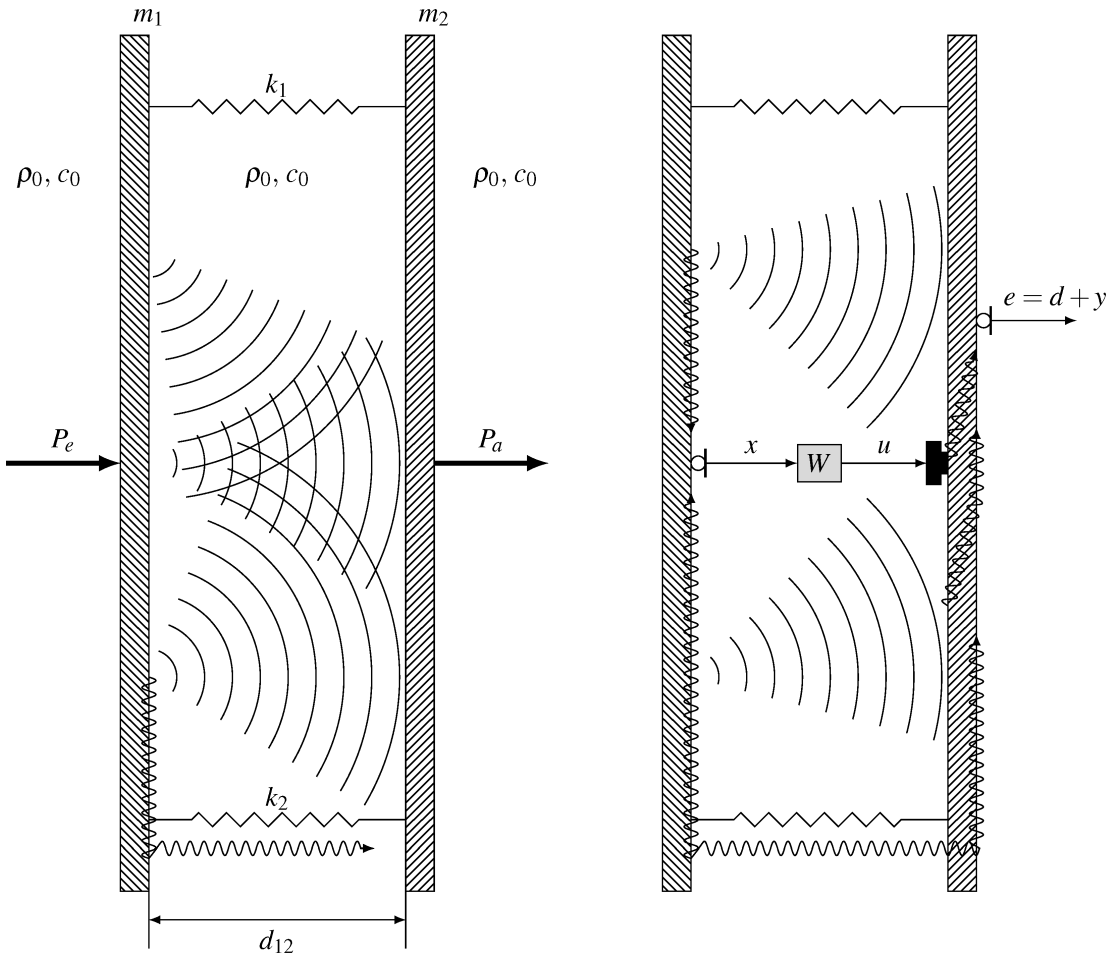

Fig. 3 – Vibro-acoustic quantities (left) and signals and components of an active feedforward control system of a double panel system (right)

The right part of Fig. 3 shows the relevant signals and components of an active FFC system which is based on the interference of structure-borne sound (AVC, ANVC or ASAC). For the sake of clarity, a single reference (SR) single input and single output (SISO) system is considered. The reference sensor, which is mounted on the primary panel, captures some (filtered) disturbance source information and provides a reference signal x to the control filter W. The control filter generates a control signal u and feeds it (amplified) to the actuator. The interference of structure-borne sound induced by the actuator and structure-borne sound originating from the disturbance source is captured by the error sensor. It provides an error signal e, which results from the superposition of the disturbance signal d and the actuator signal y. Based on the error signal (generally more than one), a vibro-acoustic performance metric is formulated, which is used for the design or the adaptation of the control filter. A control filter for an AVC system is typically designed with regard to the sum of the mean square values of the error signals[13] (p. 239). For the design of an ANVC or an ASAC system, the error signals are filtered through an acoustic filter (e.g. a sound radiation resistance matrix[14]) in order to get an acoustically relevant performance metric for the filter design. Efficient approaches are described in Elliott and Johnson[14] and in Gibbs et al.[15].

The fundamental requirement of all structure-based control systems is the directed interference of structure-borne sound. For a broadband disturbance, this can only be achieved if the active system is fast enough (ideally causal) and, in the case of an active FFC system, if the coherence of reference and disturbance signals is sufficiently high (> 90% for a reduction > 10 dB). The parameters causality and coherence will be discussed in more detail in Section 3.3. Previously, the general setup of an active FFC system and the characteristics of the considered active single and double panel systems will be described.

3.2 System

Figure 4 shows a block diagram of an active FFC system with K reference sensors, M actuators and L error sensors.

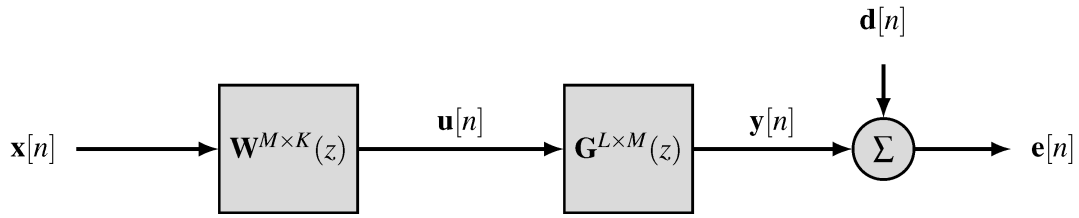

Fig. 4 –Block diagram of an active feedforward control system with K reference sensors, M actuators and L error sensors

The secondary path $\mathbf{G}$ describes the dynamics between the reference signals $\mathbf{x}$ and the error signals $\mathbf{e}$ for the special case $\mathbf{W} = \mathbf{E}$ (i.e., for the case of a trivial control filter). $\mathbf{G}$ includes the transfer functions from the actuators to the error sensors, the dynamics of the analog low-pass filters and the delays of the digital signal processing (DSP) systems. The finite impulse response (FIR) filters of the controller $\mathbf{W}$ are calculated according to Elliott[13] (p. 237ff.). The benefits of this method are the causality of the control filter, the freely selectable number of filter weights and the consideration of control effort during filter design.

Figure 5 shows a schematic top view of the considered generic active single or double panel system. The clearance of the double panel system (cp. d_{12} in Figure 3) is equal to 15 cm. The panel material is aluminum with a thickness of 2 mm. The panels are assumed to be simply supported at the edges. It is assumed that the structural damping of the panels can be approximated by a viscous modal damping ratio of 1% and that the damping of the air enclosed in the cavity between the two panels of the double panel system can be approximated by a viscous modal damping ratio of 0,0022%. The structural coupling of the panels of the double panel system is neglected because of the dominance of the airborne transmission path at low frequencies.

The disturbance excitation of the (primary) panel is realized by ten uncorrelated stochastic point forces. The disturbance source information is captured by means of ten reference sensors located at the positions of the disturbance point forces. The post-processing of the reference signals follows the procedure described in the Sections 3.1 and 3.2. The actuators and error sensors of the multiple reference (MR) multiple input and multiple output (MIMO) FFC system are collocated. This minimizes the secondary path runtime of the individual actuator-sensor-pairs. Since the whole setup of the system is generic, it provides general insight but it must be adjusted to the individual application scenario.

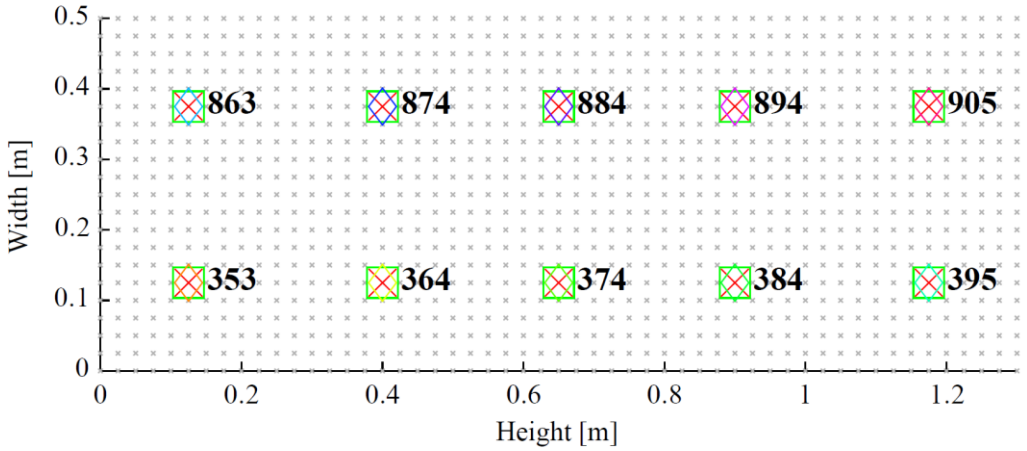

Fig. 5 – Top view of a single or a double panel system with 10 disturbance sources (red crosses), 10 reference sensors (colored hashes) and 10 collocated actuator/sensor pairs (green squares)

In order to investigate the influence of signal processing delays on the disturbance rejection of the active system, an artificial secondary path runtime of 1 ms to 5 ms (in steps of 1 ms) is introduced into the secondary path.

Table 1 – Parameters of the digital signal processing

Parameter	Value
FIR filter length (cp. Elliott[13] p. 237ff.)	$I = 1000$
Regularization factor (ditto)	$\beta = 10^{-5}$
Number of frequency lines	$N_{DFT} = 2I = 2000$
Overlap	50%
Window	Hamming
Sampling frequency	$F_s = 1000\,\mathrm{Hz}$

3.3 Influencing factors

The disturbance rejection of an active FFC is strongly influenced by the coherence of the sensor signals and by the causality of the active system. Whereas the linear dependency of reference and disturbance signals can be quantified by means of the coherence function, a universal measure of causality is not available. This work therefore proposes a new definition of a so-called causality margin.

A connection between the disturbance rejection of an active FFC, the coherence and the causality is obtained from the power spectral density (PSD) function of the error signal S_{ee}[16] (p. 57).

$$S_{ee}(f) = \left[1 - |\gamma_{\tilde{x}d}(f)|^2\right] S_{dd}(f) + \left| W(f) - \frac{S_{\tilde{x}d}(f)}{S_{\tilde{x}\tilde{x}}(f)} \right|^2 S_{\tilde{x}\tilde{x}}(f). \tag{8}$$

The first summand on the right hand side of Equation (8) accounts for the influence of the sensor signals' coherence and the second summand quantifies the impact of causality on the error signals' PSD. The first summand is determined by the coherence function of the filtered (through the secondary path) reference signal $\tilde{x}$ and the disturbance signal d. The complex coherence function of two arbitrary signals x and y depends on the cross power spectral density (CPSD) function S_{xy} and the PSD functions S_{xx} und S_{yy} [17].

$$\gamma_{xy}(f) := \frac{S_{xy}(f)}{\sqrt{S_{xx}(f)S_{yy}(f)}} \tag{9}$$

If more than one reference sensor is used, the multiple coherence function $C_{\mathbf{x}y}$ can be evaluated[13] (p. 244).

$$C_{\mathbf{x}y}(f) := \frac{\mathbf{S}_{xy}(f)\mathbf{S}_{xx}^{-1}(f)\mathbf{S}_{xy}^{H}(f)}{S_{yy}(f)} \tag{10}$$

The analysis of the implications of the coherence on the disturbance rejection of an active FFC in the case of spatially weakly correlated disturbances (e.g. a diffuse sound field or a turbulent boundary layer) is provided in the publication of Misol et al.[18].

The second summand on the right hand side of Equation (8) accounts for the causality. There, W denotes the frequency response function (FRF) of the physically realizable (causal) controller and $S_{\tilde{x}d}/S_{\tilde{x}\tilde{x}}$ is the FRF of the optimal (generally non-causal) control filter. If the active FFC is causal, both FRFs are identical and the second term vanishes. The term causality margin (CM) permits a quantification of the causality of an active FFC.

$$CM = 10\log_{10}\left(r_{ee,\mathrm{PEF}}[0]r_{ee}^{-1}[0]\right) = L_{ee,\mathrm{PEF}} - L_{ee}\ \mathrm{dB} \tag{11}$$

In Equation (11), $r_{ee,\mathrm{PEF}}[0]$ is the mean square value of the error signal of a so-called single-point delay prediction error filter (PEF)[19] and $r_{ee}[0]$ is the mean square value of the error signal of the active FFC under consideration. Generally $r_{xx}[0]$ denotes the autocorrelation function of a signal x evaluated at zero. Since the error signal of a PEF is by definition white noise, it provides an upper bound on the disturbance rejection of a non-causal active FFC. This makes the mean square value of the error signal of the PEF a suitable benchmark for the quantification of causality. If the disturbance rejection of the active FFC under consideration exceeds the one of the PEF, it must be causal (because it is able to reduce the power of a random signal). In this case CR is positive. In the opposite case, when the active FFC is non-causal, the CR is negative. The magnitude of CR provides a measure of the degree of (non-)causality.

3.4 Results

This section provides a comparison of the disturbance rejections and the CMs of active single (cp. Table 2) and active double panel systems (cp. Table 3). The coherence will not be discussed, because the considered systems are linear and all disturbance sources are captured. For a detailed analysis of the influence of the coherence on the disturbance rejection of an active FFC see Misol et al.[18]

Table 2 provides the disturbance rejection (the difference of the sum of the mean square values of the disturbance and the error signals) and the CM of the active single panel system in dependency of the secondary path runtime. The corresponding spectral representations of the disturbance rejection (difference of the summed PSDs of the error and disturbance signals) are shown in Fig. 6. As expected, larger secondary path runtimes are associated with smaller disturbance rejections and smaller CMs. According to Table 2, all CMs are negative, which implies that all active single panel systems with FFC are non-causal. This is due to the fact that the locations of the reference and the error sensors are identical. This renders the active FFC systems into active FBC system which are non-causal by definition.

Table 2 – Disturbance rejection and causality margin of a point-force-excited active single panel system for different secondary path runtimes

Secondary path runtime [ms]	Disturbance rejection [dB]	Causality margin [dB]
1	11.8	-3.5
2	10	-5.3
3	9.5	-5.8
4	9.1	-6.2
5	8.5	-6.8

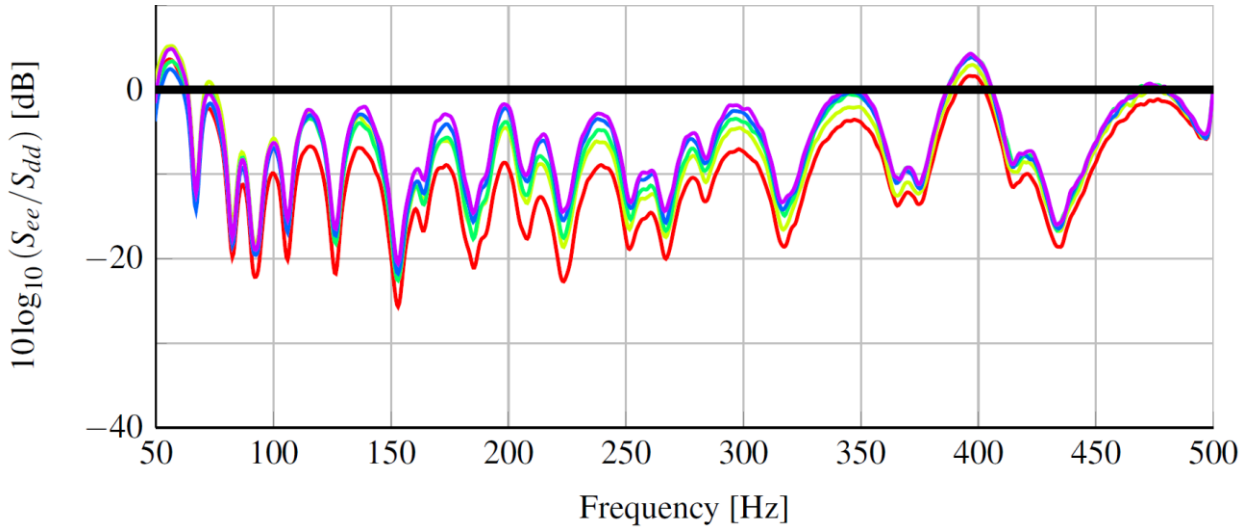

Fig. 6 –Mean Disturbance rejection of the active single panel system (10 error sensors) for different secondary path runtimes (cp. Table 2)

Table 3 and Fig. 7 provide the disturbance rejections and the CMs of the active double panel system. Obviously, the disturbance rejections are significantly increased compared to the active single panel systems whereas the CMs are basically unchanged. This is due to the increased disturbance rejection of the PEF. Hence, the increased disturbance rejections of the active double panel system are determined by the system itself and not by the causality. It seems that the spatial separation of the reference and the error sensors plays a minor part for the causality. The spatial separation of the reference sensors and the actuators (which are collocated to the error sensors) is, however, of practical relevance, because it attenuates the feedback path. This leads to an increase in robustness and performance of the active FFC system. According to the CMs, the active double panel system is rather insensitive to an increase in the secondary path runtime.

Altogether, the disturbance rejections of the active double panel systems exceed the ones of the active single panel systems by more than 10 dB.

Table 3 – Disturbance rejection and causality margin of a point-force-excited active double panel system dependent on the secondary path runtime

Secondary path runtime [ms]	Disturbance rejection [dB]	Causality margin [dB]
1	23.6	-3.9
2	23.4	-4.1
3	23	-4.6
4	22	-5.6
5	21.3	-6.2

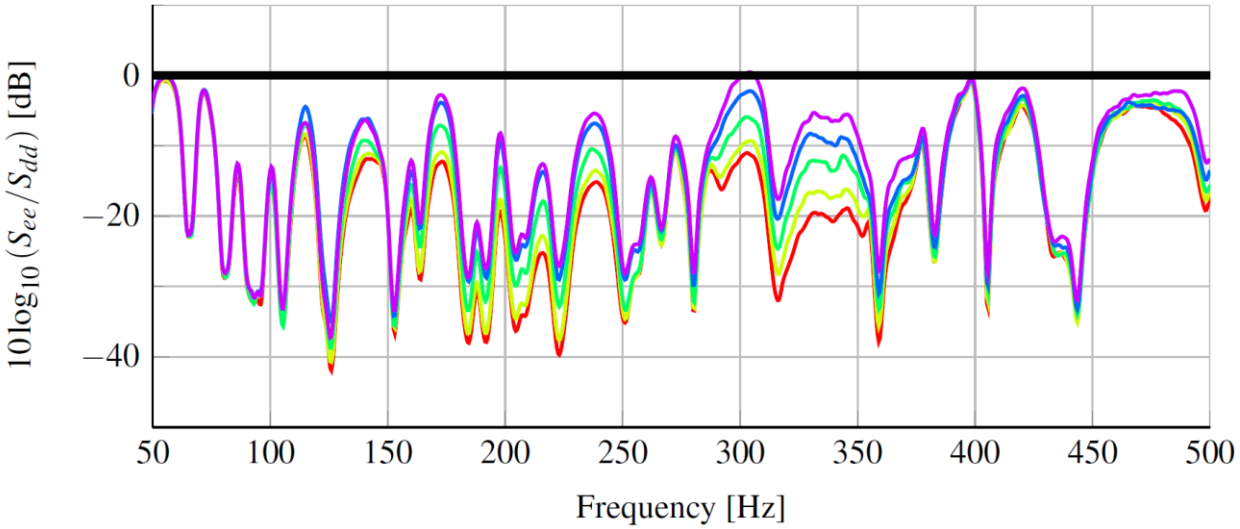

Fig. 7 –Mean Disturbance rejection of the active double panel system (10 error sensors) for different secondary path runtimes (cp. Table 3)

4 SUMMARY AND CONCLUSION

This contribution motivates the application of broadband active feedforward control in automobiles. It focuses on the transmission of broadband disturbances through single or double panel systems (e.g. the combination of roof skin and liner). A discussion of the mechanisms of sound transmission through panel structures reveals the limitations of passive sound insulation methods on the one hand and demonstrates the potential of active noise reduction systems at low frequencies on the other hand. Subsequently, the influencing of the sound transmission by means of active feedforward control is presented and the parameters coherence and causality are described. Terms and methods for the analysis of the coherence and the causality of active feedforward control systems are introduced and applied to simulation models of generic single and double panel systems. The simulation results show a significantly increased disturbance rejection of the active double panel system compared to the active single panel system. Whereas the active single panel system achieves a maximum disturbance rejection of 11.8 dB, the maximum disturbance rejection of the active double panel systems amounts to 23.6 dB. Similar results are reported for higher damping values of the structures and the cavity (see Misol[20]).

6 REFERENCES

1. S. J. Elliott. A review of active noise and vibration control in road vehicles. Technical Report 981, University of Southampton, 2008.
2. T. J. Sutton, S. J. Elliott, A. M. McDonald, and T. J. Saunders. Active control of road noise inside vehicles. *Noise Control Engineering Journal*, 42(4):137–147, July 1994.
3. H. Sano, T. Inoue, A. Takahashi, K. Terai, and Y. Nakamura. Active control system for low-frequency road noise combined with an audio system. *IEEE Transactions on Speech and Audio Processing*, 9(7):755–763, 2001.
4. Jordan Cheer. *Active control of the acoustic environment in an automobile cabin*. PhD thesis, University of Southampton, December 2012.
5. S. H. Oh, H. S. Kim, and Y. J. Park. Active control of road booming noise in automotive interiors. *The Journal of the Acoustical Society of America*, 111(1):180–188, January 2002.
6. W. Dehandschutter and P. Sas. Active control of structure-borne road noise using vibration actuators. *Journal of Vibration and Acoustics, Transactions of the ASME*, 120(2):517–523, 1998.
7. Tom Weyer, Elmar Breitbach, and Olaf Heintze. Self-tuning active electromechanical absorbers for tonal noise reduction of a car roof. In *INTER-NOISE - International Congress and Exhibition on Noise Control Engineering*, Istanbul, Turkey, August 2007.
8. M. Misol, S. Algermissen, and H. P. Monner. Experimental investigation of different active noise control concepts applied to a passenger car equipped with an active windshield. *Journal of Sound and Vibration*, 331(10):2209–2219, 2012.
9. F. Fahy and P. Gardonio. *Sound and Structural Vibration: Radiation, Transmission and Response*. Academic Press, Oxford/Burlington, 2. edition, 2007.
10. S. A. Hambric and J. B. Fahnline. Structural acoustics tutorial – part ii: Sound-structure interaction. *Acoustics Today*, 3(2):9–27, 2007.
11. Stephan Tewes. *Active Trim Panel Attachments for Control of Sound Transmission through Aircraft Structures*. PhD thesis, Technische Universität München, München, 2006.
12. Paolo Gardonio and Stephen John Elliott. Active control of structure-borne and airborne sound transmission through double panel. *Journal of Aircraft*, 36(6):1023–1032, 1999.
13. S. J. Elliott. *Signal Processing for Active Control*. Academic Press, London, 2001.
14. S. J. Elliott and M. E. Johnson. Radiation modes and the active control of sound power. *The Journal of the Acoustical Society of America*, 94(4):2194–2204, 1993.
15. Gary P. Gibbs, Robert L. Clark, David E. Cox, and Jeffrey S. Vipperman. Radiation modal expansion: Application to active structural acoustic control. *The Journal of the Acoustical Society of America*, 107(1):332–339, 2000.
16. S. M. Kuo and D. Morgan. *Active Noise Control Systems: Algorithms and DSP Implementations*. John Wiley & Sons, Inc., New York, 1996.
17. G. Clifford Carter. Coherence and time delay estimation. *Proceedings of the IEEE*, 75(2):236–255, 1987.
18. Malte Misol, Christian Bloch, Hans Peter Monner, and Michael Sinapius. Performance of active feedforward control systems in non-ideal, synthesized diffuse sound fields. *The Journal of the Acoustical Society of America*, 135(4):1887–1897, 2014.
19. J. G. Cook and S. J. Elliott. Connection between multichannel prediction error filter and spectral factorisation. *IEE Electronics letters*, 35(15):1218–1220, 1999.
20. Malte Misol. *Aktive Steuerung des Transmissionsverhaltens stochastischer Störquellen durch flächige Leichtbaustrukturen [Active feedforward control of the transmission of stochastic disturbances through lightweight panel structures]*. Dlr-forschungsbericht, Technische Universität Carolo-Wilhelmina zu Braunschweig, Köln, Deutschland, 2014.